0026-895X/07/7201-132–140
MOLECULAR PHARMACOLOGY
U.S. Government work not protected by U.S. copyright
Mol Pharmacol 72:132–140, 2007

Vol. 72, No. 1
34876/3225054
Printed in U.S.A.

Identification and Characterization of a New Tubulin-Binding Tetrasubstituted Brominated Pyrrole

Susan L. Mooberry, Kimberly N. Weiderhold, Sivanesan Dakshanamurthy, Ernest Hamel, Edith J. Banner, Anastasia Kharlamova, Jonathan Hempel, John T. Gupton, and Milton L. Brown

Department of Physiology and Medicine, Southwest Foundation for Biomedical Research, San Antonio, Texas (S.L.M., K.N.W.); Lombardi Comprehensive Cancer Center, Drug Discovery Program, Department of Oncology, Georgetown University Medical Center, Washington DC (S.D., M.L.B.); Toxicology and Pharmacology Branch, Developmental Therapeutics Program, Division of Cancer Treatment and Diagnosis, National Cancer Institute at Frederick, National Institutes of Health, Frederick, Maryland (E.H.); and Department of Chemistry, Gottwald Center for the Sciences, University of Richmond, Richmond, Virginia (E.J.B., A.K., J.H., J.T.G.)

Received February 6, 2007; accepted April 17, 2007

ABSTRACT

We studied the mechanism of action of 3,5-dibromo-4-(3,4-dimethoxyphenyl)-1*H*-pyrrole-2-carboxylic acid ethyl ester (JG-03-14) and found that it is a potent microtubule depolymerizer. JG-03-14 caused a dose-dependent loss of cellular microtubules, formation of aberrant mitotic spindles, accumulation of cells in the G_2/M phase of the cell cycle, and Bcl-2 phosphorylation. These events culminated in the initiation of apoptosis, as evidenced by the caspase 3-dependent cleavage of poly(ADP-ribose) polymerase (PARP). JG-03-14 has antiproliferative activity against a wide range of cancer cell lines, with an average IC_{50} value of 62 nM, and it is a poor substrate for transport by P-glycoprotein. JG-03-14 inhibited the polymerization of purified tubulin in vitro, consistent with a direct interaction between the compound and tubulin. JG-03-14 potently inhibited the binding of [^{3}H]colchicine to tubulin, suggesting that it bound to tubulin at a site overlapping the colchicine site. JG-03-14 had antitumor effects in the PC3 xenograft model, in which it caused greater than 50% reduction in tumor burden after 14 days of treatment. Molecular modeling studies indicated that the dimethoxyphenyl group of JG-03-14 occupies a space similar to that of the trimethoxyphenyl group of colchicine. However, the 2,3,5-trisubstituted pyrrole group, which is connected to the dimethoxyphenyl moiety, interacted with both α and β tubulin in space not shared with colchicine, suggesting significant differences compared with colchicine in the mechanism of binding to tubulin. Our results suggest that this tetrasubstituted pyrrole represents a new, biologically active chemotype for the colchicine site on tubulin.

Microtubules are cellular structures that play a central role in metabolism, intracellular transport, and cell division. A wide range of chemicals have been identified that interrupt microtubule function. These compounds can be divided into microtubule stabilizers and microtubule depolymerizers. Microtubule stabilizers include paclitaxel, discodermolide, the epothilones, and the laulimalides. Microtubule stabilizers cause an increase in the density of cellular microtubules, and they stimulate the assembly of purified tubulin. In contrast, microtubule depolymerizers cause a loss of cellular microtubules, and they inhibit the assembly of purified tubulin. Microtubule depolymerizing compounds can be further subdivided into those that bind to tubulin within the colchicine site and those that bind within the vinca domain. Agents acting upon the colchicine site include 2ME2, combretastatin A-4, and podophyllotoxin. The phenotypic effects of microtubule stabilizing and depolymerizing agents are quite disparate when they are used at high concentrations in cells, but at their lowest antiproliferative concentrations, both classes of agents inhibit microtubule dynamics (Jordan and Wilson, 2004). In due course, inhibition of microtubule dynamics is believed to hinder the normal function of the mitotic spindle,

This work was supported by grants from the William Randolph Hearst Foundation, the Amon Carter Foundation (to S.L.M.) and the National Institutes of Health Area Program R15-CA67236 (to J.T.G.).
Article, publication date, and citation information can be found at http://molpharm.aspetjournals.org.
doi:10.1124/mol.107.034876.

ABBREVIATIONS: 2ME2, 2-methoxyestradiol; Pgp, P-glycoprotein; PDB, Protein Database; DMA-colchicine, *N*-deacetyl-*N*-(2-mercaptoacetyl)-colchicine; RMSD, root mean square difference; MD, molecular dynamics; FBS, fetal bovine serum; SRB, sulforhodamine B; RR, relative resistance; PARP, poly(ADP-ribose) polymerase; DMSO, dimethyl sulfoxide; R123, rhodamine 123; $DiOC_2(3)$, 3′-diethyloxacarbocyanine iodide; NCI, National Cancer Institute.

leading to mitotic arrest and initiation of apoptosis (Jordan and Wilson, 2004).

Drugs that target microtubules have an important role in the treatment of cancer. Paclitaxel and docetaxel are among the most effective drugs used to treat ovarian, breast, head and neck, and lung cancers. The vinca alkaloids, vinblastine, vincristine, and newer generation analogs, such as vinorelbine, are used in the treatment of a wide range of childhood and adult tumors. Several new tubulin binding drugs are being evaluated in clinical trials, including 2ME2 and combretastatin A-4 phosphate. It is noteworthy that these two agents seem to bind within the same binding site on tubulin, the colchicine site, yet they have very different effects on tumor vasculature. 2ME2 has well-described antiangiogenic actions (Mooberry, 2003), whereas combretastatin A-4 phosphate has antivascular activities that lead to rapid collapse of tumor vasculature (Griggs et al., 2001). How these differential effects are mediated is not yet understood, but such knowledge may lead to the development of newer-generation colchicine site agents.

Natural products containing pyrrole have diverse and interesting biological activities, and they have proven to be particularly useful as lead compounds for drug development (Gupton, 2006). As part of our long-term program to develop vinylogous iminum salt-based syntheses of natural products containing the pyrrole group, some early synthetic intermediates were evaluated against tumor cell lines (Burnham et al., 1998). Many of these compounds were highly active against cancer cells, and some inhibited DNA synthesis without binding directly to DNA (Gupton et al., 1999). Earlier studies also provided clues to the design of pyrrole analogs that might have potent antiproliferative activities and the ability to bind to tubulin. The marine natural product lukianol A contains a highly oxygenated 3,4-diphenylpyrrole motif, and it potently inhibited the growth of the human KB cancer cell line (Yoshida et al., 1992). Banwell and colleagues (1997) suggested that lukianol A represented a configurationally stable hybrid of combretastatin A-4 and colchicine. We have synthesized another class of biologically interesting pyrroles, which are somewhat related to the pyrrolomycin natural products by virtue of their halogenated pyrrole backbone (Charan et al., 2006). Brominated analogs of previously synthesized pyrroles were prepared, and they retained the cytotoxic activity exhibited by the nonbrominated pyrroles (Gupton et al., 2000). Whereas mechanistic studies indicated that two of the brominated pyrrole compounds bound directly to DNA, causing DNA cross-linking, the mechanisms of action of other brominated pyrrole analogs remained unknown. Based on the structural similarity of the compounds to combretastatin A-4 and Banwell's suggestion that several pyrrole containing natural products represent stable hybrids of combretastatin and colchicine, we examined the effects of these brominated pyrroles on cellular microtubules. Several of the brominated pyrrole analogs had microtubule-depolymerizing effects. The most potent was JG-03-14 (structure shown in Fig. 1). JG-03-14 is structurally unique among combretastatin-like compounds. It possesses a single highly oxygenated phenyl group; other combretastatin analogs always possess two highly oxygenated phenyl groups. The mechanisms of action of JG-03-14 were evaluated, and it was found to be a potent antimitotic agent. Binding studies show that JG-03-14 binds to tubulin within the colchicine site. Modeling studies suggest that JG-03-14 represents a novel chemotype for the colchicine site. Our studies indicate that this compound has antitumor effects, and it represents a promising lead for the generation of new analogs with important biological properties.

Materials and Methods

Synthesis of JG-03-14. JG-03-14 was synthesized as described previously (Gupton et al., 2000).

Cell Culture. MDA-MB-435 cancer cells were obtained from the Lombardi Cancer Center of Georgetown University (Washington, DC). The NCI/ADR cell line was obtained from NCI (Frederick, MD). This cell line was previously called the MCF7/ADR cell line, but the name was changed when it was determined that the cell line was not derived from MCF-7 cells (Scudiero et al., 1998). The cancer cell lines HeLa, PC3, and DU145 and the A-10 embryonic rat vascular smooth muscle cell line were purchased from the American Type Culture Collection (Manassas, VA). MDA-MB-435 and DU145 cells were grown in IMEM Richter's medium (BioSource International, Camarillo, CA) with 10% FBS (Hyclone, Logan, UT) and 25 μg/ml gentamicin sulfate. A-10 and HeLa cells were grown in basal medium Eagle containing Earle's salts, 50 μg/ml gentamicin sulfate, and 10% FBS. PC3 and NCI/ADR cells were grown in RPMI 1640 (BioSource International) containing 50 μg/ml gentamicin sulfate and 10% FBS.

Growth Inhibition Assay. The SRB assay was used to measure the antiproliferative effects of JG-03-14 (Skehan et al., 1990; Boyd and Paull, 1995). Cells were placed in 96-well plates at predetermined densities and allowed to attach and grow for 24 h. The test compounds were then added and allowed to incubate with the cells for 48 h. IC_{50} values were calculated as described previously (Tinley et al., 2003b).

Pgp Efflux Assay. Cell-based functional assays were used to evaluate the ability of JG-03-14 to inhibit the efflux of the Pgp substrates R123 or $DiOC_2(3)$ from NCI/ADR cells using the protocol outlined in the Chemicon multidrug resistance direct dye efflux kit (Chaudhary and Roninson, 1991; Minderman et al., 1996). NCI/ADR cells (2×10^6 cells/ml) were incubated with 1 μg/ml $DiOC_2(3)$ for 15 min or with 10 μg/ml R123 for 30 min in ice-cold RPMI 1640 media with 1% bovine serum albumin in the dark to load the fluorescent dye into the cells. Dye efflux dependent on Pgp is temperature-dependent, so an aliquot kept on ice provided a control for maximal loading. Another aliquot of cells warmed to 37°C for 15 min without test compound was used as a positive control for Pgp-mediated dye efflux. This treatment resulted in a dramatic reduction in intracellular fluorescence as measured by flow cytometry. The inclusion of 2.2 μM vinblastine in an aliquot of cells provided a positive control for a known Pgp substrate that dramatically inhibited the efflux of each of the fluorescent substrates. $DiOC_2(3)$ and R123 loaded cells were also incubated with 5, 10, or 20 μM JG-03-14, and dye efflux was evaluated by flow cytometry. Propidium iodide was used as a counterstain in all cell aliquots.

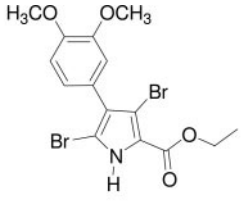

3,5 dibromo-4-(3,4-dimethoxyphenyl)-1*H*-pyrrole-2-carboxylic acid ethyl ester

(JG-03-14)

Fig. 1. Structure of 3,5-dibromo-4-(3,4-dimethoxyphenyl)-1*H*-pyrrole-2-carboxylic acid ethyl ester (JG-03-14).

Indirect Immunofluorescence. The effects of JG-03-14 on mitotic and interphase microtubules and nuclear structures were examined in A-10 vascular smooth muscle cells and in HeLa cells. The cells were treated for 18 to 24 h with a range of concentrations of JG-03-14, and then the cells were fixed and microtubules visualized using a β-tubulin antibody as described previously (Tinley et al., 2003b). Centrosomes were visualized using a γ-tubulin antibody, and 4′,6-diamidino-2-phenylindole was used to visualize DNA.

Cell Cycle Analysis. The effects of JG-03-14 on cell cycle distribution were evaluated using flow cytometry. MDA-MB-435 cells in log phase growth were treated with 50 to 75 nM JG-03-14 for 24 h. The cells were harvested, stained with Krishan's reagent (Krishan, 1975), and analyzed with a FACScan flow cytometer (BD Biosciences, San Jose, CA). Instrument linearity was checked using quality control samples. The cell cycle distribution data are presented as propidium iodide intensity versus the number of events.

Western Blotting. MDA-MB-435 cells in log phase growth were treated for 24 h with 75 nM JG-03-14. Cells were lysed in cell lysis buffer (BioSource) with protease inhibitors. Cell lysates containing equal amounts of protein were separated by polyacrylamide gel electrophoresis, and protein expression was determined by Western blotting techniques. The Bcl-2 antibody was obtained from BD Biosciences, and the p85 cleaved PARP antibody was purchased from Promega (Madison, WI).

Tubulin Assembly in Vitro. The ability of JG-03-14 to alter tubulin assembly was evaluated in a glutamate-based tubulin assembly system. The reactions were conducted with purified bovine brain tubulin (1.0 mg/ml; 10 μM), 0.8 M monosodium glutamate, pH 6.6, 0.4 mM GTP, and 4% (v/v) DMSO, with and without several concentrations of JG-03-14, combretastatin A-4, or thiocolchicine. Reaction mixtures were incubated for 15 min at 30°C without GTP to allow drug binding. The mixtures were put on ice, GTP was added, and the reaction mixtures were transferred to cuvettes and held at 0°C to establish baselines. After baselines were established, the mixtures were warmed to 30°C, and turbidity was monitored at 350 nm as described previously (Hamel, 2003). Combretastatin A-4 was kindly provided by Dr. G. R. Pettit, Arizona State University, and thiocolchicine by Dr. A. Brossi, National Institute of Diabetes and Digestive and Kidney Diseases (Bethesda, MD).

Inhibition of Colchicine Binding. The effects of JG-03-14 on colchicine binding to purified tubulin were evaluated using a DEAE-cellulose filtration assay (Borisy, 1972; Verdier-Pinard et al., 1998). The reaction mixtures contained 1 μM purified bovine brain tubulin, 5% (v/v) DMSO, 5 μM [^{3}H]colchicine, and a range of concentrations of JG-03-14, combretastatin A-4, or thiocolchicine.

Antitumor Evaluations. The in vivo antitumor effects of JG-03-14 were evaluated in a murine xenograft model using human prostate PC3 cells. Six-week-old male nude mice (athymic NCr nu/nu, homozygous; NCI) were injected unilaterally subcutaneously in the flank with 1.3×10^6 PC3 cells mixed 50:50 with Matrigel (Matrigel Basement Membrane Matrix; BD Biosciences) in 100-μl volumes. The mice were monitored for 8 days after implantation for tumor development. When tumors reached 0.2 to 0.5 cm^3, mice were randomly divided into control and treatment groups. Mice in the treatment group were injected intraperitoneally with 200 mg/kg JG-03-14 in a volume of 50 μl. This concentration was selected based on dose-tolerance testing. Twelve treatments were given over 18 days, for a total dose of 2400 mg/kg. JG-03-14 was solubilized in DMSO. Mice in the control group received 50 μl of DMSO per injection. The trial was terminated on day 19 after treatment initiation.

Molecular Modeling and Docking Studies. The X-ray crystal structure of two α,β-tubulin heterodimers complexed with DMA-colchicine and a stathmin fragment (PDB: 1SA0) was used for the automated molecular docking of JG-03-14. Inconsistencies between the PDB format and the tubulin residues library translation to atomic potential types were corrected manually. Tubulin was minimized using the DISCOVER (Accelrys, San Diego, CA) program's cff91 force field (Maple et al., 2004) with distance-dependent dielectrics.

Molecular Docking and Minimization. At first, the JG-03-14 ligand was constructed using SYBYL7.0 (Tripos, Inc., St. Louis, MO) and optimized with MP2/6-31G** basis set using the Gaussian 03 quantum mechanical program (Frisch et al., 2003). Docking experiments were performed with the AutoDock 3.0.5 (Morris et al., 1999) and FlexX programs (Rarey et al., 1996). In general, standard docking procedures were used. In the case of AutoDock, the torsion angles for a protein and ligand were identified for 10 independent runs per ligand. A grid of $60 \times 60 \times 60$ points on the x, y, and z axes was built, centered on the center of the mass of the JG-03-14 N atom in the tubulin active site. A grid spacing of 0.4 Å and a distance-dependent function of the dielectric constant were used for calculation of the energetic map. The default settings were used for all other parameters. At the end of the docking simulation, ligands with the most favorable free energy of binding were selected as the best structures for the ligand-tubulin complex. In the case of FlexX, all the parameters were used as in default settings, except that the number of solution conformations was set to 90.

The best docked geometry for JG-03-14 was minimized using the DISCOVER module of Insight II (Accelrys). A consistent valence force field (cff91) was used. The cutoff for nonbonded interaction energies was set to infinity (i.e., no cutoff) with the dielectric constant set at 4 to account for the dielectric shielding found in proteins. Each minimization was carried out in two steps, first using steepest descent minimization for 200 cycles and then using conjugate gradient minimization until the average gradient fell below 0.01 kcal/mol. All atoms within 6.0 Å of the inhibitor were allowed to relax during the minimization, whereas those atoms beyond 6.0 Å were held rigid.

Molecular Dynamics Simulations. The minimized complex was subjected to molecular dynamics simulations using the DISCOVER module of Insight II (Accelrys Inc.). Molecular dynamics simulations performed in the NVE ensemble consisted of an initial equilibration of 25 ps followed by a production run of 300 ps dynamics at 300 K. The final complex structure at the end of the molecular dynamics simulation was subjected to 2000 steps of steepest descent energy minimization followed by conjugate gradient energy minimization. A distance-dependent dielectric constant and nonbonded distance cutoff of 12 Å were used. Molecular dynamics simulations were also performed using the AMBER 8 package (Case, 2004) with the general amber force field (Wang et al., 2004) and RMSD charge models (Bayly et al., 1993).

Results and Discussion

A series of tetrasubstituted brominated pyrroles were synthesized as part of a strategy for the preparation of halogenated pyrroles based on natural products including the lukianols, lamellarins, ningalins, polycitones, and pyrrolomycins. These compounds were evaluated for microtubule disrupting effects, and JG-03-14 was found to have potent microtubule depolymerizing activity. Earlier studies showed that JG-03-14 had potent antiproliferative effects against mouse and human leukemia cell lines (Gupton et al., 2000).

JG-03-14 Inhibits the Growth of Cancer Cell Lines and Evades P-Glycoprotein-Mediated Drug Resistance. The antiproliferative effects of JG-03-14 were evaluated in several cancer cell lines, including a multidrug resistant cell line, NCI/ADR, that has a high level of expression of Pgp. Representative dose-response curves for the MDA-MB-435 cell line, which has negligible levels of Pgp, and the NCI/ADR line are shown in Fig. 2. The results show that both cell lines were very sensitive to the antiproliferative and cytotoxic effects of JG-03-14. Average IC_{50} values of 35.5 and 59.3 nM were obtained for JG-03-14 in the MDA-MB-435 and

NCI/ADR cell lines, respectively (Table 1). A RR value of 1.7 was calculated by dividing the IC_{50} value of the multidrug resistant cell line NCI/ADR by the IC_{50} value of the MDA-MB-435 cell line. The 1.7 RR value indicates that JG-03-14 is a poor substrate for transport by Pgp. Paclitaxel (Taxol), a well-known substrate for Pgp, has an RR value in these cell lines of 827 to 4050 (Tinley et al., 2003b; Weiderhold et al., 2006). Further studies to evaluate the ability of JG-03-14 to be a substrate for Pgp-mediated transport were conducted using the NCI/ADR cell line. A flow cytometry-based assay was used to evaluate the ability of JG-03-14 to inhibit the efflux of two Pgp substrates, R123 and $DiOC_2(3)$. In contrast to vinblastine, a known Pgp substrate, 5 to 20 μM JG-03-14 did not inhibit the efflux of either fluorescence Pgp substrate. These data, together with the proliferation results in the NCI/ADR cells, offer convincing evidence that JG-03-14 is a poor substrate for transport by Pgp.

The antiproliferative effects of JG-03-14 were evaluated in three other cancer lines, and the IC_{50} values are shown in Table 1. The data indicate that JG-03-14 had potent antiproliferative activity against a range of tumor types, including prostate cancer cell lines. JG-03-14 was also evaluated in the NCI 60 cell line panel, and these studies showed that JG-03-14 had broad antiproliferative and cytotoxic activities against a wide range of cancer cell types. Non–small-cell lung cancer cell lines and renal cancer cell lines were some of the most sensitive in the NCI evaluation (data not shown). JG-03-14 is a structurally novel pyrrole-derivative that has potent antiproliferative actions against a wide range of cancer cell lines, and it has advantages over other tubulin-binding drugs in its ability to circumvent Pgp-mediated drug resistance.

Effects of JG-03-14 on Interphase and Mitotic Microtubules. The effects of JG-03-14 on cellular microtubules were evaluated in cell-based phenotypic assays. JG-03-14 caused loss of interphase microtubules in A-10 cells and the formation of structurally aberrant mitotic spindle structures. The effects of JG-03-14 on interphase microtubules are shown in Fig. 3. A-10 cells were used to investigate the effects of antimitotic drugs on interphase microtubule structures because, unlike cancer cells, vascular smooth muscle cells largely arrest in the G_1 stage of the cell cycle after treatment with tubulin-binding antimitotic agents (Blagosklonny et al., 2004). Vehicle-treated cells exhibited a normal array of interphase microtubules that nucleate from the microtubule organizing centers in the vicinity of the nucleus (Fig. 3A). Treatment of the cells with JG-03-14 caused a concentration-dependent loss of interphase microtubules. Microtubule loss was first noted at the cell periphery in cells treated with 250 nM JG-03-14 (Fig. 3B). In cells treated with 500 nM JG-03-14, there was a much greater loss of interphase microtubules. At this concentration, a few short microtubule remnants remained at the periphery of the cell, with more microtubules in the region surrounding the nucleus (Fig. 3C). A 1 μM concentration of JG-03-14 caused essentially total loss of cellular microtubules, and yet the cell size was unchanged, as occurs with other microtubule depolymerizers (Fig. 3D). A second common characteristic observed with compounds that bind to tubulin is their ability to induce micronucleation. This also occurred with JG-03-14 treatment. Examples of such cells are shown in Fig. 3, B and C, in which the outline of the normal rounded nuclei or abnormal segmented micronuclei can be seen.

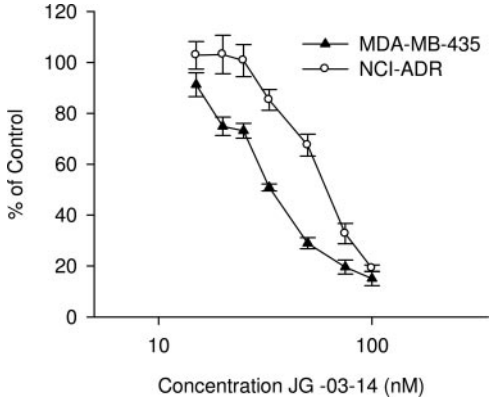

Fig. 2. Antiproliferative effects of JG-03-14 in cell lines with negligible and high levels of Pgp. The antiproliferative effects of JG-03-14 were measured using the SRB assay. The data represent the means of three experiments ± S.E.

In addition to disrupting interphase microtubules, microtubule-depolymerizing agents cause the formation of abnormal mitotic spindles (Tinley et al., 2003a; Weiderhold et al., 2006). The effects of JG-03-14 on mitotic spindles were evaluated in HeLa cells. These cells arrest in the G_2/M phase of the cell cycle in response to tubulin-targeting antimitotic agents. HeLa cells were treated for 18 h with a range of concentrations of JG-03-14, and microtubules, centrosomes, and DNA were visualized (Fig. 4). In vehicle-treated cells, normal bipolar spindles radiating from centrosomes containing γ-tubulin were observed (Fig. 4A). In JG-03-14-treated cells, a variety of abnormal mitotic spindle structures was seen, including cells with multipolar mitotic spindles (Fig. 4B). Among other aberrant mitotic spindles were circular spindles (Fig. 4C) that typically occurred in pairs within single cells. Abnormal mitotic spindles were also observed in A-10 cells (data not shown). Such abnormal spindles indicate that JG-03-14 probably interferes with normal mitotic progression.

JG-03-14 Causes Accumulation of Cells in G_2/M, Phosphorylation of Bcl-2, and PARP Cleavage. A common effect of microtubule depolymerizing agents is their ability to cause mitotic arrest by interrupting mitosis at the metaphase to anaphase transition. The visualization of highly aberrant mitotic spindles and the accumulation of cells in metaphase suggested that JG-03-14 inhibited mitotic progression. This was confirmed by measuring the effects of JG-03-14 on cell cycle distribution. MDA-MB-435 cells were treated with a range of concentrations of JG-03-14 for 24 h.

TABLE 1

Antiproliferative effects of JG-03-14 as determined by the SRB assay

The IC_{50} values were calculated from the linear portions of the log dose response curve for each of three experiments conducted, and the average values obtained are presented ± S.D. The relative resistance value was calculated by dividing the IC_{50} value of the drug-resistant cell line, NDI/ADR, by the IC_{50} value of the drug-sensitive cell line, MDA-MB-435.

Cell Type	IC_{50}
	nM
MDA-MB-435	35.5 ± 0.16
NCI/ADR	59.3 ± 3.2
HeLa	54.7 ± 4.7
PC3	79.6 ± 0.68
DU145	76.6 ± 2.2
Relative resistance value	1.67

The DNA content of vehicle-treated cells is shown in the top left of Fig. 5A. G_2/M accumulation was apparent in cells treated with 50 nM JG-03-14, and a dose-dependent increase in G_2/M accumulation occurred with 60 and 75 nM concentrations. An abnormal, wide G_1 peak was observed in cells treated with 50 and 60 nM JG-03-14. This peak has been referred to as an aneuploid G_1 peak, and it occurs in cells treated with low concentrations of microtubule stabilizers (Chen and Horwitz, 2002) and some microtubule-depolymerizing agents (Weiderhold et al., 2006). At slightly higher concentrations, there was no evidence of any G_1 peak, and most of the cells were in the G_2/M phase of the cell cycle. These data confirm that JG-03-14 inhibits mitotic progression.

In addition to causing mitotic arrest, microtubule-interacting agents initiate the phosphorylation of the antiapoptotic protein Bcl-2 (Haldar et al., 1997). The ability of JG-03-14 to cause Bcl-2 phosphorylation was studied. Treatment of cells with 75 nM JG-03-14 caused the appearance of increasing amounts of slower-migrating forms of Bcl-2, consistent with its phosphorylation. The ability of JG-03-14 to initiate apoptosis was evaluated by the appearance of the p85-cleaved form of PARP. Full-length PARP is cleaved by activated caspase 3 to form the p85 protein fragment. A 24-h incubation of MDA-MB-435 cells with 75 nM JG-03-14 caused a large increase in the density of cleaved p85 PARP, consistent with early activation of caspase 3 apoptosis pathways. The ability of compounds to cause Bcl-2 phosphorylation and initiation of caspase-dependent apoptosis are hallmarks of tubulin-binding antimitotic compounds. The ability of JG-03-14 to cause microtubule depolymerization, mitotic arrest, Bcl-2 phosphorylation, and initiation of apoptosis are consistent with a tubulin-binding antimitotic mechanism of action.

JG-03-14 Inhibits the Assembly of Purified Tubulin and [^{3}H]Colchicine Binding to Tubulin. To test the hypothesis that JG-03-14 binds to tubulin, the effects of JG-03-14 on purified tubulin polymerization were studied in an in vitro tubulin assembly system. JG-03-14 caused a concentration-dependent inhibition of tubulin assembly, with an IC_{50} value for inhibiting tubulin assembly of 1.5 μM (Table 2). These data show that JG-03-14 at substoichiometric concentrations is a potent inhibitor of tubulin polymerization.

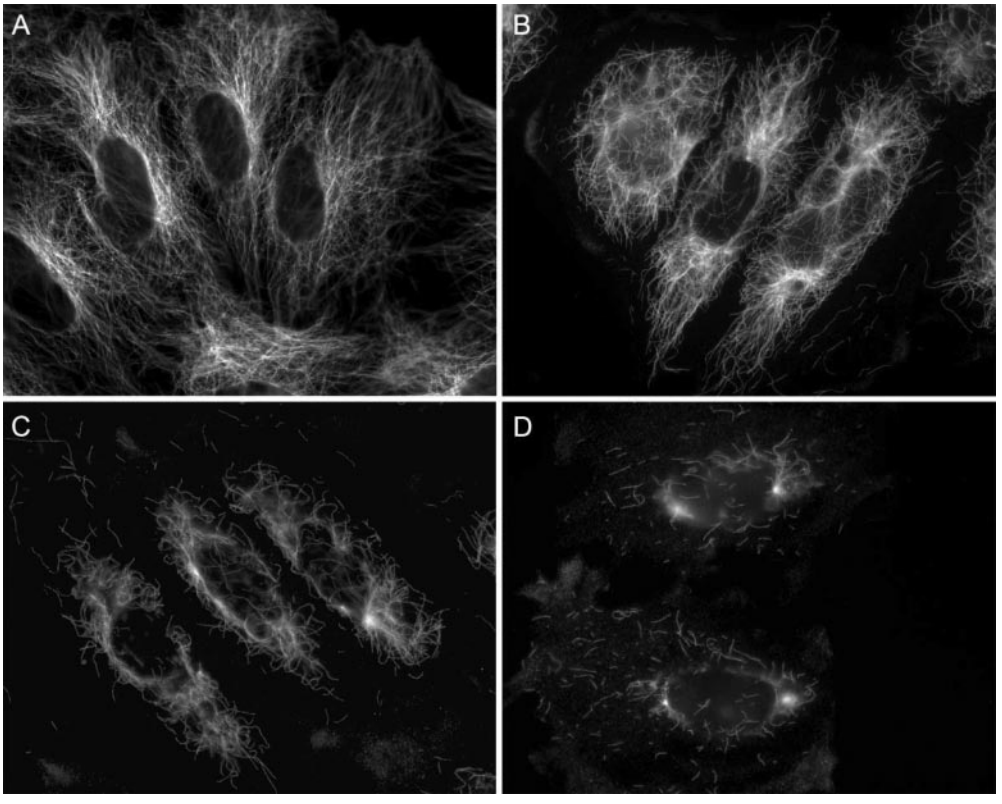

Fig. 3. JG-03-14 causes interphase microtubule loss. The effects of JG-03-14 on cellular microtubules were evaluated using indirect immunofluorescence techniques in A-10 cells treated with DMSO (A), or JG-03-14 at 250 nM (B), 500 nM, (C) or 1 μM (D).

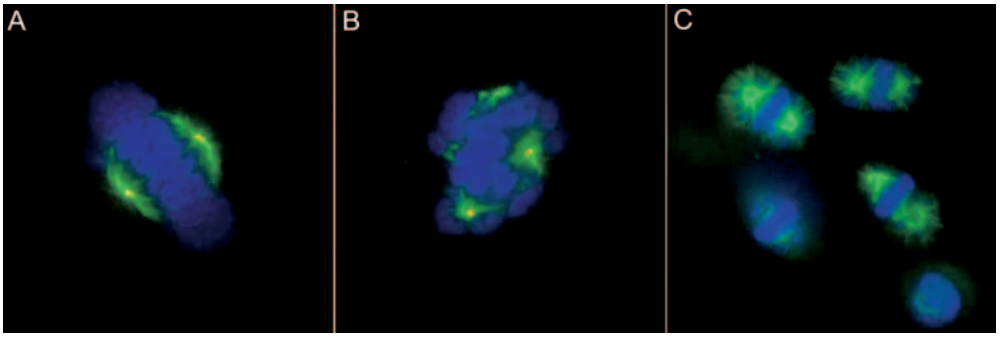

Fig. 4. Effects of JG-03-14 on mitotic spindles. HeLa cells were treated with a range of concentrations of JG-03-14 for 18 h, and microtubules were visualized with a β-tubulin antibody, centrosomal structures were visualized with a γ-tubulin antibody and DNA with 4′,6-diamidino-2-phenylindole. Cells were treated with vehicle (A) or 10 nM JG-03-14 (B and C).

The potency of JG-03-14 for inhibition of tubulin assembly was comparable with that observed with two well-known microtubule-depolymerizing agents, combretastatin A-4 and thiocolchicine. These data confirm the conclusion from the cellular studies that the antimitotic activity of JG-03-14 results from a direct interaction of the compound with tubulin and that JG-03-14 acts as a microtubule-depolymerizing agent.

The binding site of JG-03-14 on tubulin was investigated by demonstrating that JG-03-14 potently inhibited the binding of [^{3}H]colchicine to tubulin. As shown in Table 2, JG-03-14 was somewhat more potent than thiocolchicine and somewhat less potent than combretastatin A-4 as an inhibitor of colchicine binding. Previous studies have shown that both combretastatin A-4 and thiocolchicine bind to the colchicine site on tubulin (Lin et al., 1989). These data suggest that JG-03-14 binds to tubulin within a site that overlaps the colchicine binding site. The compound has activity as an inhibitor of assembly and of colchicine binding comparable with that of the highly potent agents combretastatin A-4 and thiocolchicine.

In Vivo Antitumor Activity of JG-03-14. JG-03-14 was a potent and effective inhibitor of cancer cell proliferation in vitro. Therefore, studies were initiated to determine whether it had antitumor effects. A human PC3 xenograft model was used, in part because this cell line was sensitive to the antiproliferative effects of JG-03-14. Tumor cells were implanted in a mixture of Matrigel, and, when the tumors were large enough to be palpable, the mice were randomized into control and treatment groups. Mice in the treatment group were treated 12 times over a period of 18 days for a total dose of JG-03-14 of 2400 mg/kg. Mice in the control group received vehicle. The results demonstrate that systemic treatment of the mice with JG-03-14 caused a marked reduction in the size of the tumors measured at 14 days compared with the vehicle-treated group (Fig. 6). These results show that JG-03-14 has antitumor effects and that it should be further evaluated for antitumor actions.

JG-03-14 represents a new pharmacophore that can be further explored to improve upon its biological properties and to probe the colchicine-binding site. New compounds will be designed to optimize tubulin binding and to improve aqueous solubility. Better aqueous solubility will provide for more flexibility for in vivo administration and testing.

Molecular Modeling of the Binding Mode of JG-03-14 to Tubulin. Molecular modeling studies, with automated docking simulations, were conduced to further explore the interaction between tubulin and JG-03-14. These studies produced several potential binding conformations of JG-03-14. We compared all low-energy conformations of JG-03-14 generated in our studies with the bound conformation of DMA-colchicine from the crystal structure (PDB: 1SA0). One molecular conformation of JG-03-14 was notably closer to the DMA-colchicine conformation within the binding site (Fig. 7; JG-03-14 carbons are depicted in white, and DMA-colchicine carbons in green). It is interesting that in this model, the three-dimensional arrangement of the dimethoxyphenyl group of JG-03-14 occupies a space similar to that of the trimethoxyphenyl group of the bound DMA-colchicine. This overlapping ensemble was buried in the α,β-tubulin struc-

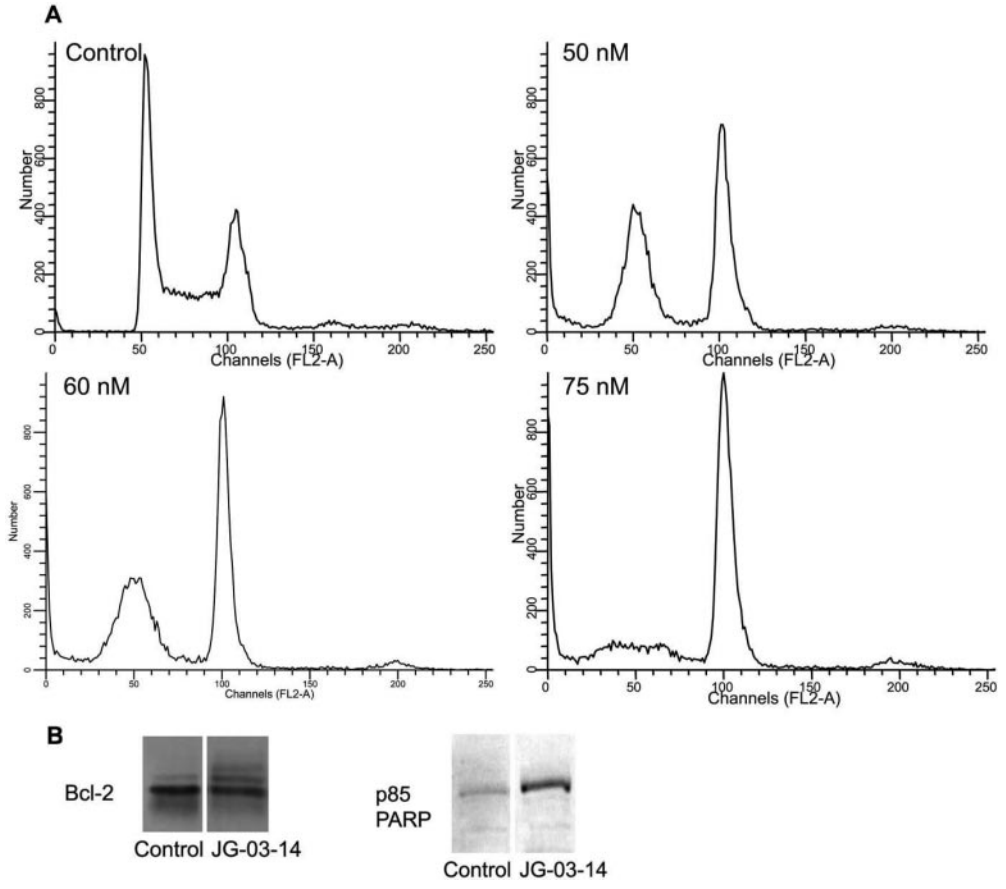

Fig. 5. JG-03-14 causes mitotic accumulation, Bcl-2 phosphorylation, and PARP cleavage. MDA-MB-435 cells in log phase growth were treated with vehicle or 50 to 75 nM JG-03-14 for 24 h, and the cell cycle distribution of the cells was measured using flow cytometry (A). The flow cytometry data are presented as propidium iodide intensity versus number of events. For Western blots, MDA-MB-435 cells were treated for 24 h with 75 nM JG-03-14 and cell lysates made. Equal amounts of protein were separated by polyacrylimide gel electrophoresis and transferred onto Immobilon P membranes. The membranes were probed with specific antibodies, as indicated, for Bcl-2 (B) and cleaved PARP (C).

ture near the Cys-β241 residue (Fig. 8). The docking procedure was validated by comparing the binding mode obtained by docking known tubulin polymerization inhibitors, including DMA-colchicine, podophyllotoxin, and combretastatin A-4. The results were quantified in terms of both lowest estimated energy of binding and RMSD between the binding conformation predicted by our model and others reported previously (Uppuluri et al., 1993; Bai et al., 1996; Nogales et al., 1998; Ravelli et al., 2004; Kong et al., 2005; Lawrence and McGown, 2005). In our docking simulations using AutoDock and FlexX, we found that the dimethoxyphenyl moiety of JB-03-14 was positioned similarly to that of the trimethoxyphenyl group of DMA-colchicine with an RMSD deviation of 0.35 and 0.66 Å, respectively. Finally, we selected the binding mode predicted by AutoDock that was within 0.35 Å of the trimethoxyphenyl group of DMA-colchicine.

Docking putative inhibitors in a rigid protein binding site derived from a complex with another ligand may not predict the correct binding mode. Furthermore, ligand binding can cause a wide range of induced conformational changes in the amino acid side chains of the protein. Thus, we further refined the binding mode of JG-03-14 using MD simulations. At first, the tubulin-JG-03-14 complex was subjected to energy minimization to relieve any unfavorable interactions. The minimized structure was then used as the initial input for a MD simulation run of 300 ps, performed in the NVE ensemble. Because the α,β-tubulin heterodimer is large, during the simulation, residues within 20 Å of the ligand were allowed to move, whereas all other residues were fixed. Low-energy minimum structures were collected every 10 ps, giving a total of 30 structures that were energy-minimized, and these were further analyzed. To evaluate the readjustment of the active site residues in the calculated tubulin-JG-03-14 complexes, the RMSD between the atoms of the original tubulin-JG-03-14 complex and the corresponding atoms of each calculated tubulin-JG-03-14 complex was determined. In the case of backbone atoms' superimposition, the RMSD was lower than 0.5 Å, whereas for side chains, the maximum RMSD

TABLE 2
JG-03-14 inhibits tubulin assembly and [^{3}H]colchicine binding to tubulin

The effects of JG-03-14, combretastatin A-4, and thiocolchicine on tubulin assembly were studied. IC_{50} values for inhibition were determined and are presented ± S.D. The effects of these compounds on [^{3}H]colchicine binding were determined using 5 μM [^{3}H]colchicine and 1 μM tubulin. Percentage of inhibition ± S.D. is presented. Combretastatin A-4 and thiocolchicine represent positive controls for both assays. At least two experiments were performed in both assays with each compound.

	Inhibition of Tubulin Assembly (10 μM Tubulin)	Inhibition of [^{3}H]Colchicine Binding	
		1 μM	5 μM
	μM	%	
JG-03-14	1.5 ± 0.2	49 ± 3	84 ± 0.6
Combretastatin A-4	1.3 ± 0.08	83 ± 2	97 ± 2
Thiocolchicine	1.0 ± 0.1	N.D.	67 ± 0.07

N.D., not determined.

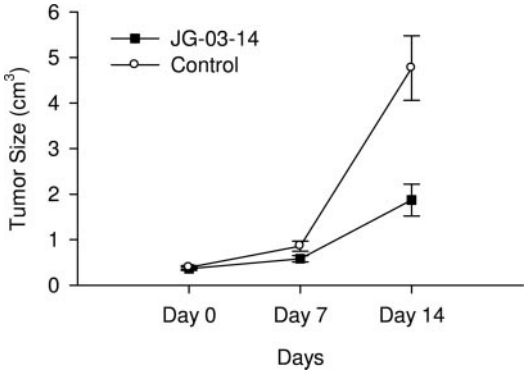

Fig. 6. Antitumor effects of JG-03-14 in a PC3 xenograft model. The efficacy of JG-03-14 in a human prostate tumor was evaluated in a human xenograft model. PC3 cells were mixed with Matrigel and then implanted unilaterally into the flank of male nude mice. After tumors had developed, the mice were randomly assigned to treatment and control groups. Each mouse in the treatment group (n = 14) received a total dose of 2400 mg/kg JG-03-14 over 18 days. The compound was administered via intraperitoneal injections. Twelve treatments were given. Control mice (n = 11) were treated with the vehicle.

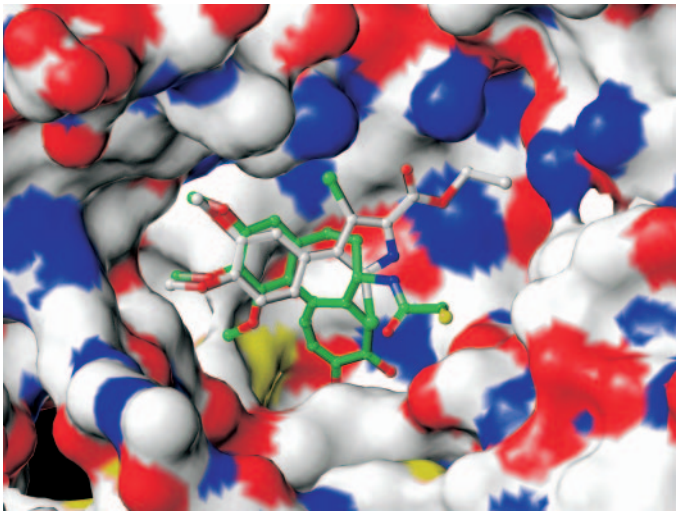

Fig. 7. Root mean square fit of JG-03-14 (carbon atoms colored white) with DMA- colchicine (carbon atoms colored green) inside the colchicine binding site. α,β-Tubulin is represented by the electrostatic potential surface (red atoms for negatively charged amino acids and blue atoms for positively charged amino acids; yellow represents sulfur). In the two ligands, oxygen atoms are shown in red, nitrogen in blue, sulfur in yellow, and the bromine atoms of JG-03-14 in green.

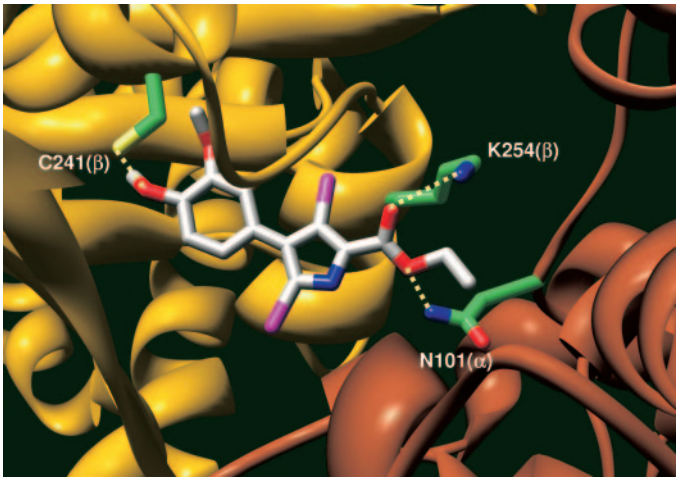

Fig. 8. JG-03-14 bound to α,β-tubulin. The image shows a binding model of JG-03-14 with both α-tubulin (colored brown) and β-tubulin (colored yellow). The polypeptide backbones are rendered as ribbons. Interactive residue side chains at the colchicine site (Cys-β241, Lys-β254, and Asn-α101) and JG-03-14 are shown in stick rendering, with the carbon atoms of tubulin colored green and the carbon atoms of the JG-03-14 colored white. The yellow broken lines indicate potential intermolecular hydrogen bonds. Oxygen atoms are shown in red, bromine in magenta, nitrogen in blue, and sulfur in yellow.

found was approximately 1.1 Å. These data show that ligand-induced conformational changes were small and more pronounced for side chains than for the polypeptide backbone. Finally, the global energy minimum of the 30 collected structures was selected as the preferred binding model.

Analyses of the 30 lowest-energy minima of JG-03-14 docked in the crystal structure revealed a potential H-bond formed with Cys-β241 (residue numbering as in Ravelli et al., 2004) and the dimethoxyphenyl moiety of the ligand. There is also an H-bond in the starting complex structure between the carbonyl group of JG-03-14 and Asn-α101. During the course of the MD simulations, a resonating form representing a bifurcated H-bond with two amino hydrogens of Asn-α101 was revealed. Furthermore, in the initial docking model, the dimethoxyphenyl group of JG-03-14 did not form a H-bond with Lys-β254. However after MD a H-bond was observed between Lys-β254 and the oxygen atom of the dimethoxyphenyl group of JG-03-14. This suggests that, although ligand-induced conformational changes are small, such changes can be critical to the protein active site side chains during ligand binding. In the final model shown in Fig. 8, the hydrogen bonds between JG-03-14 and tubulin are as follows: 1) the dimethoxyphenyl group is hydrogen-bonded to the thiol group of Cys-β241; 2) the carbonyl oxygen is hydrogen bonded to the terminal NH of Lys-β254; and 3) the JG-03-14 side chain ethoxy oxygen forms a bifurcated H-bond interaction with the NH_2 of Asn-α101. We noticed that the molecular elements of the ligand connected to dimethoxyphenyl group of JG-03-14 were positioned in a slightly different location in the binding site than the molecular elements of DMA-colchicine relative to the trimethoxyphenyl group. This is due to the planar nature of the JG-03-14 compound; the differing positions in the binding site were also the result of the specific groups attached to the dimethoxyphenyl moiety. We also observed that dimethoxyphenyl moiety was buried well inside the hydrophobic pocket containing Val238, Cys241, Leu242, Leu248, Ala250, Leu255, Ala317, Val318, and Ala354 of β-tubulin. As shown in Fig. 8, the 4-methoxy oxygen of the dimethoxyphenyl group engages in hydrogen bonding to the Cys-β241 SH group. The methyl groups of the dimethoxyphenyl moiety are oriented so that favorable hydrophobic interactions occur with the side chains of β-tubulin residues Val238, Leu242, Leu248, Ala250, Leu255, Ala317, Val318, and Ala354 located above and below the plane of the phenyl ring. These interactions of the dimethoxyphenyl group of JG-03-14 are similar to the interactions with tubulin of the trimethoxyphenyl moiety of DMA-colchicine. This provides a reasonable explanation for the similarities between the antimicrotubule activity of JG-03-14 in comparison with that of thiocolchicine. However, the disubstituted pyrrole of JG-03-14 attached to the dimethoxyphenyl moiety interacts differently with tubulin than do rings B and C and the C-7 side chain of DMA-colchicine, and these structural elements interact with both the α and β polypeptide chains. Furthermore, JG-03-14 is a planar compound, and its dimethoxyphenyl moiety has a slight tilt of 13° relative to the trimethoxyphenyl moiety of DMA-colchicine. The existence of small empty pockets on tubulin closer to the disubstituted pyrrole moiety of JG-03-14 than to DMA-colchicine might allow for an improvement in the interactions between pyrrole derivatives and vacant regions of the binding site (Fig. 7), depending on specific substituents. The volume and topography of these empty pockets in the colchicine site shown in Fig. 7 provide an opportunity to modify and optimize the substituent groups of the pyrrole for shape, size, and polarity to maximize the interaction of ligands with the molecular surface of tubulin. These molecular models will therefore be used to design new analogs of JG-03-14 to optimize interactions with tubulin.

Detailed docking and in silico modeling studies indicate that the interaction of JG-03-14 with tubulin has unique features, and this provides a novel view of how small molecule inhibitors can interact within the colchicine site on tubulin. The JG-03-14 binding model identifies new portions of the tubulin heterodimer that may interact with small molecules to disrupt microtubule actions. JG-03-14 represents a new scaffold to use for the design and synthesis of compounds that might have promising biological activities. Use of analogs with slightly different binding properties might also help decipher differences in the biological activities of various colchicine site agents. In particular, studies with JG-03-14 and related compounds might provide important answers as to the nature of the differences that colchicine site agents show in their antimitotic, antiangiogenic, and antivascular effects. Perhaps nuances in binding mechanisms initiate varying downstream effects that culminate in different cellular responses.

Acknowledgments

We extend special thanks to Patrice M. Hills and Erin A. Clark for help in many aspects of this project. We acknowledge supporting contributions from Marya Dunlap-Brown in the MAPS core at the University of Virginia and the Drug Discovery Program at Georgetown University Medical Center. We acknowledge the National Cancer Institute for allocation of computing time and staff support at the Advanced Biomedical Computing Center of the National Cancer Institute, Frederick, Maryland.

References

Bai R, Pei XF, Boye O, Getahun Z, Grover S, Bekisz J, Nguyen NY, Brossi A, and Hamel E (1996) Identification of cysteine 354 of β-tubulin as part of the binding site for the A ring of colchicine. *J Biol Chem* **271:**12639–12645.

Banwell MG, Flynn BL, Hamel E, and Hockless DCR (1997) Convergent synthesis of the pyrrolic marine natural products lamellarin-O, lamellarin-Q, lukianol-A and some more highly oxygenated congeners. *Chem Commun* **2:**207–208.

Bayly C, Cieplak P, Cornell WD, and Kollman PA (1993) A well-behaved electrostatic potential based method using charge restraints for deriving atomic charges: the RESP model. *J Phys Chem* **97:**10269–10280.

Blagosklonny MV, Darzynkiewicz Z, Halicka HD, Pozarowski P, Demidenko ZN, Barry JJ, Kamath KR, and Herrmann RA (2004) Paclitaxel induces primary and postmitotic G1 arrest in human arterial smooth muscle cells. *Cell Cycle* **3:**1050–1056.

Borisy GG (1972) A rapid method for quantitative determination of microtubule protein using DEAE-cellulose filters. *Anal Biochem* **50:**373–385.

Boyd MR and Paull KD (1995) Some practical considerations and applications of the National Cancer Institute in vitro anticancer discovery screen. *Drug Dev Res* **34:**91–109.

Burnham BS, Gupton JT, Krumpe K, Webb T, Shuford J, Bowers B, Warren AE, Barnes C, and Hall IH (1998) Cytotoxicity of substituted alkyl-3,4-bis(4-methoxyphenyl)pyrrole-2-carboxylates in L1210 lymphoid leukemia cells. *Arch Pharm (Weinheim)* **331:**337–341.

Case DA, Darden TA, Cheatham TE III, Simmerling CL, Wang J, Duke RE, Luo R, Merz KM, Wang B, Pearlman DA, et al. (2004) AMBER 8. University of California at San Francisco, San Francisco.

Charan RD, Schlingmann G, Bernan VS, Feng X, and Carter GT (2006). Dioxapyrrolomycin biosynthesis in *Streptomyces fumanus*. *J Nat Prod* **69:**29–33.

Chaudhary PM and Roninson IB (1991) Expression and activity of P-glycoprotein, a multidrug efflux pump, in human hematopoietic stem cells. *Cell* **66:**85–94.

Chen JG and Horwitz SB (2002) Differential mitotic responses to microtubule-stabilizing and -destabilizing drugs. *Cancer Res* **62:**1935–1938.

Frisch MJ, Trucks GW, Schlegel HB, Scuseria GE, Robb MA, Cheeseman JR, Montgomery JA Jr, Vreven T, Kudin KN, Burant JC, et al. (2003) Gaussian 03. Gaussian, Inc., Pittsburgh, PA.

Griggs J, Metcalfe JC, and Hesketh R (2001) Targeting tumour vasculature: the development of combretastatin A4. *Lancet Oncol* **2:**82–87.

Gupton JT (2006) Pyrrole natural products with antitumor properties, in *Heterocy-*

clic Antitumor Antibiotics: Topics in Heterocyclic Chemistry (Lee M ed) pp 53–92, Springer-Verlag, Berlin.
Gupton JT, Burham BS, Byrd BD, Krumpe KE, Stokes C, Shuford J, Winkle S, Webb T, Warren AE, Barnes CR, et al. (1999) The cytotoxicity and mode of action of 2,3,4-trisubstituted pyrroles and related derivatives in human Tmolt4 leukemia cells. *Pharmazie* **54:**691–697.
Gupton JT, Burham BS, Krumpe K, Du K, Sikorski JA, Warren AE, Barnes CR, and Hall IH (2000) Synthesis and cytotoxicity of 2,4-disubstituted and 2,3,4-trisubstituted brominated pyrroles in murine and human cultured tumor cells. *Arch Pharm (Weinheim)* **333:**3–9.
Haldar S, Basu A, and Croce CM (1997) Bcl2 is the guardian of microtubule integrity. *Cancer Res* **57:**229–233.
Hamel E (2003) Evaluation of antimitotic agents by quantitative comparisons of their effects on the polymerization of purified tubulin. *Cell Biochem Biophys* **38:**1–22.
Jordan MA and Wilson L (2004) Microtubules as a target for anticancer drugs. *Nat Rev Cancer* **4:**253–265.
Kong Y, Grembecka J, Edler MC, Hamel E, Mooberry SL, Sabat M, Rieger J, and Brown ML (2005) Structure-based discovery of a boronic acid bioisostere of combretastatin A-4. *Chem Biol* **12:**1007–1014.
Krishan A (1975) Rapid flow cytofluorimetric analysis of mammalian cell cycle by propidium iodide staining. *J Cell Biol* **66:**188–193.
Lawrence NJ and McGown AT (2005) The chemistry and biology of antimitotic chalcones and related enone systems. *Curr Pharm Des* **11:**1679–1693.
Lin CM, Ho HH, Pettit GR, and Hamel E (1989) Antimitotic natural products combretastatin A-4 and combretastatin A-2: studies on the mechanism of their inhibition of the binding of colchicine to tubulin. *Biochemistry* **28:**6984–6991.
Maple J, Hwang M-J, Stockfisch T, Dinur U, Waldman M, Ewig C, and Hagler A (2004) Derivation of class II force fields. I. Methodology and quantum force field for alkyl functional group and alkane molecules. *J Comput Chem* **15:**162–182.
Minderman H, Vanhoefer U, Toth K, Yin MB, Minderman MD, Wrzosek C, Slovak ML, and Rustum YM (1996) DiOC2(3) is not a substrate for multidrug resistance protein (MRP)-mediated drug efflux. *Cytometry* **25:**14–20.
Mooberry SL (2003) New insights into 2-methoxyestradiol, a promising antiangiogenic and antitumor agent. *Curr Opin Oncol* **15:**425–430.
Morris G, Goodsell D, Halliday R, Huey R, Hart W, Belew R, and Olson A (1999) Automated docking using a Lamarckian genetic algorithm and an empirical binding free energy function. *J Comput Chem* **19:**1639–1662.
Nogales E, Wolf SG, and Downing KH (1998) Structure of the alpha beta tubulin dimer by electron crystallography. *Nature* **391:**199–203.
Rarey M, Kramer B, Lengauer T, and Klebe G (1996) A fast flexible docking method using an incremental construction algorithm. *J Mol Biol* **261:**470–489.
Ravelli RB, Gigant B, Curmi PA, Jourdain I, Lachkar S, Sobel A, and Knossow M (2004) Insight into tubulin regulation from a complex with colchicine and a stathmin-like domain. *Nature* **428:**198–202.
Scudiero DA, Monks A, and Sausville EA (1998) Cell line designation change: multidrug-resistant cell line in the NCI anticancer screen. *J Natl Cancer Inst* **90:**862.
Skehan P, Storeng R, Scudiero D, Monks A, McMahon J, Vistica D, Warren JT, Bokesch H, Kenney S, and Boyd MR (1990) New colorimetric cytotoxicity assay for anticancer-drug screening. *J Natl Cancer Inst* **82:**1107–1112.
Tinley TL, Leal RM, Randall-Hlubek DA, Cessac JW, Wilkens LR, Rao PN, and Mooberry SL (2003a) Novel 2-methoxyestradiol analogues with antitumor activity. *Cancer Res* **63:**1538–1549.
Tinley TL, Randall-Hlubek DA, Leal RM, Jackson EM, Cessac JW, Quada JC Jr, Hemscheidt TK, and Mooberry SL (2003b) Taccalonolides E and A: plant-derived steroids with microtubule-stabilizing activity. *Cancer Res* **63:**3211–3220.
Uppuluri S, Knipling L, Sackett DL, and Wolff J (1993) Localization of the colchicine-binding site of tubulin. *Proc Natl Acad Sci U S A* **90:**11598–11602.
Verdier-Pinard P, Lai JY, Yoo HD, Yu J, Marquez B, Nagle DG, Nambu M, White JD, Falck JR, Gerwick WH, et al. (1998) Structure-activity analysis of the interaction of curacin A, the potent colchicine site antimitotic agent, with tubulin and effects of analogs on the growth of MCF-7 breast cancer cells. *Mol Pharmacol* **53:**62–76.
Wang J, Wolf R, Caldwell J, Kollman P, and Case D (2004) Development and testing of a general amber force field. *J Comput Chem* **25:**1157–1174.
Weiderhold KN, Randall-Hlubek DA, Polin LA, Hamel E, and Mooberry SL (2006) CB694, a novel antimitotic with antitumor activities. *Int J Cancer* **118:**1032–1040.
Yoshida WY, Lee KK, Carroll AR, and Scheuer PJ (1992) A complex pyrrolo-oxazinone and its iodo derivative isolated from a tunicate. *Helv Chim Acta* **75:**1271–1275.

Address correspondence to: Dr. Susan L. Mooberry, Department of Physiology and Medicine, Southwest Foundation for Biomedical Research, P.O. Box 760549, San Antonio, Texas 78245-0549. E-mail: smooberry@sfbr.org